Assessing the aggregation behaviour of iron oxide nanoparticles under relevant environmental conditions using a multi-method approach

Laura Chekli[a,b], Sherub Phuntsho[a], Maitreyee Roy[c], Enzo Lombi[d], Erica Donner[b,d] and Ho Kyong Shon[a,b,*]

[a]School of Civil and Environmental Engineering, University of Technology, Sydney (UTS), Post Box 129, Broadway, NSW 2007, Australia.

[b]CRC CARE, PO Box 486, Salisbury, SA 5106, Australia

[c]National Measurement Institute Australia, Department of Industry, Innovation, Science, Research and Tertiary Education PO Box 264, Lindfield NSW 2070, Australia

[d]Centre for Environmental Risk Assessment and Remediation, University of South Australia, Building X, Mawson Lakes Campus, SA 5095, Australia

*Corresponding author: Email: Hokyong.Shon-1@uts.edu.au

Abstract

Iron nanoparticles are becoming increasingly popular for the treatment of contaminated soil and groundwater; however, their mobility and reactivity in subsurface environments are significantly affected by their tendency to aggregate. Assessing their stability under environmental conditions is crucial for determining their environmental fate. A multi-method approach (including different size-measurement techniques and the DLVO theory) was used to thoroughly characterise the behaviour of iron oxide nanoparticles (Fe_2O_3NPs) under environmentally relevant conditions. Although recent studies have demonstrated the importance of using a multi-method approach when characterising nanoparticles, the majority of current studies continue to use a single-method approach.

Under some soil conditions (i.e. pH 7, 10 mM NaCl and 2 mM $CaCl_2$) and increasing particle concentration, Fe_2O_3NPs underwent extensive aggregation to form large aggregates (> 1 µm). Coating the nanoparticles with dissolved organic matter (DOM) was investigated as an alternative "green" solution to overcoming the aggregation issue instead of using the more commonly proposed polyelectrolytes. At high concentrations, DOM effectively covered the surface of the Fe_2O_3NPs, thereby conferring negative surface charge on the particles across a wide range of pH values. This provided electrostatic stabilisation and considerably reduced the particle aggregation effect. DOM-coated Fe_2O_3NPs also proved to be more stable under high ionic strength conditions. The presence of $CaCl_2$, however, even at low concentrations, induced the aggregation of DOM-coated Fe_2O_3NPs, mainly via charge neutralisation and bridging. This has significant implications in regards to the reactivity and fate of these materials in the environment.

Keywords: Iron oxide, Nanoparticles, Aggregation, Flow Field-Flow Fractionation, DLVO Theory, Surface coating.

1. Introduction

Manufactured nanoparticles (MNPs) are defined as intentionally engineered materials with at least one dimension in the 1-100 nm size range (Lead and Wilkinson 2006). Due to their small size, they have often been shown to display improved catalytic, chemical, optical, mechanical, electronic and magnetic properties over conventional micro/macroscale particles (Jortner and Rao 2002). Over recent decades, some MNPs have attracted increasing attention due to their potential efficacy in the treatment of contaminated soil and groundwater (Crane and Scott 2012).

Due to their low cost, highly reactive surface sites and high *in-situ* reactivity, the most widely studied engineered nanoparticles for soil and groundwater remediation are nanoscale zero-valent iron (nZVI) nanoparticles (Wang and Zhang 1997; Elliott and Zhang 2001; Zhang 2003). Numerous studies have shown that the nanoparticles are highly effective for the removal/degradation or stabilisation of a wide range of common environmental contaminants including chlorinated organic solvents (Elliott and Zhang 2001; Zhang 2003), organic dyes (Liu et al. 2005), various inorganic compounds (Alowitz and Scherer 2002), and even some metals (Kanel et al. 2005). In the past few years, a variety of iron oxide nanoparticles have also been investigated for environmental remediation purposes. Despite the potential efficacy of these materials, many laboratory and pilot-scale field studies have demonstrated that the mobility and reactivity of iron-based nanoparticles are substantially limited in natural porous systems (e.g. soils and groundwater aquifers) (Schrick et al. 2004; Quinn et al. 2005; He and Zhao 2007; Saleh et al. 2007). Aggregation is considered to be the primary cause of reduced mobility and reactivity, and this phenomenon is the result of many factors including solution pH, ionic strength and the presence of organic matter (Ponder et al. 2000; Saleh et al. 2005). In the case of iron-based nanoparticles, previous studies have investigated that these nanoparticles have pH-dependant surface charges and that extensive aggregation due to charge neutralisation occurs near the point of zero charge (PZC) (Sun et al. 2006; Baalousha et al. 2008; Baalousha 2009; Hu et al. 2010). Furthermore, soil and groundwater conditions are often characterised by high ionic strength and high concentrations of monovalent (e.g., Na^+, K^+) and divalent (e.g., Ca^{2+}, Mg^{2+}) cations in the mM range; factors that are known to reduce electrostatic repulsion between particles and thereby enhance aggregation (Saleh et al. 2008).

To optimise the use of MNPs for environmental remediation it is necessary to understand the factors that cause aggregation under environmentally relevant conditions with the aim of enhancing their mobility while still maintaining good reactivity (Saleh et al. 2007). Surface modifications using charged polymers, polyelectrolytes or surfactants are now widely used to disperse nanoparticles in environmental matrices such as soil and water (Zhang et al. 1998; Schrick et al. 2004; Saleh et al. 2005; He et al. 2007; Saleh et al. 2007; Hajdú et al. 2009; Phenrat et al. 2009; Sirk et al. 2009; Cirtiu et al. 2011). These modifications can theoretically provide both electrostatic and steric (so-called electrosteric) stabilisation to prevent particles from aggregating and can also reduce the propensity for surface attachment (Saleh et al. 2005; Saleh et al. 2008). Unfortunately, although these different surface coatings can enhance nanoparticle stability, they can also be expensive, have toxic effects on the environment, and alter the interaction of MNPs with contaminants (Tiraferri et al. 2008). Natural surface coating by the adsorption of dissolved organic matter (DOM) such as humic and fulvic acids on the surface of nanoparticles has also been studied as an alternative “green” surface coating, and has been demonstrated to enhance nanoparticle stability through electrosteric stabilisation (Mylon et al. 2004; Illes and Tombácz 2006; Hu et al. 2010). The advantage of DOM over conventional

surface modifiers is that DOM is ubiquitous in the environment, cheap, non-toxic, and not only has the ability to adsorb onto metal oxide nanoparticles but is also able to complex with heavy metals (Liu et al. 2008; Dickson et al. 2012). A recent study by Chen et al. (Chen et al. 2011) demonstrated that DOM–coated nZVI may significantly mitigate bacterial toxicity due to the electrosteric hindrance preventing direct contact.

In this study, characterisation of bare Fe_2O_3NPs and the aggregation behaviour of these nanoparticles under relevant environmental conditions (i.e. pH, particle concentration and ionic strength) were performed using flow field-flow fractionation (FlFFF), dynamic light scattering (DLS) and scanning electron microscopy (SEM). Although the characterisation of MNPs can be considerably simpler than it is for natural particle samples, MNPs are also complex, and a multiple characterisation approach is necessary to ensure the accuracy of the characterisation data (Lead and Wilkinson 2006; Domingos et al. 2009). In fact, due to analytical challenges, the lack of appropriate characterisation data in environmentally realistic conditions is a major limitation of current research in this area. As such, there is clearly a need for useful characterisation tools that can assist in assessing MNP behaviour under relevant environmental conditions. Flow field-flow fractionation (FlFFF) is well suited to measuring MNP behaviour under relevant conditions simply by modifying the mobile phase used during characterisation. However, one of the main limitations of FlFFF is related to material losses during analysis. These generally occur via particle-membrane interaction and adsorption and may represent up to 50% of the injected mass (Hassellöv and Kaegi 2009). The particle-membrane interaction is mainly due to attractive forces (e.g. Van der Waals), hydrophobic and charge interactions which are all dependent on the mobile phase characteristics.

This is the first time that FlFFF has been applied to study the aggregation behaviour of Fe_2O_3NPs under relevant environmental conditions. The results have been compared with those from other size-measurement techniques and theoretical models to provide increased confidence in the outcomes. The stability of the DOM-coated Fe_2O_3NPs was also assessed under relevant conditions using FlFFF and DLS. Although many studies have demonstrated that DOM-coated Fe_2O_3NPs can be stable under a wide range of pH and NaCl concentrations, there is a lack of data in regard to the effect of divalent cations, especially Ca^{2+}, which is known to complex easily with organic matter (Hong and Elimelech 1997).

The results of this study are also relevant to the aggregation behaviour of nZVI, as nZVI particles have been shown to have substantial shells of iron oxide (Phenrat et al. 2007). Therefore, Fe_2O_3NPs demonstrate various similar properties to nZVI when they are used to treat contaminated soil and groundwater and can thus be used as a model system for understanding aggregation behaviour (He et al. 2008).

2. Theoretical method: The DLVO theory

The Derjaguin–Landau–Verwey–Overbeek (DLVO) theory (Derjaguin and Landau 1941; Verwey 1947; Verwey and Overbeek 1948) was employed in this study to model the interactions between Fe_2O_3NPs at different particle concentrations, pH and ionic strength. This theory provides the classical explanation for the stability of colloids in suspension. It states that the stability of nanoparticles can be explained by the sum (i.e. total interaction energy) of the van der Waals attractive forces (V_{vdw}) and the electrostatic repulsive forces (V_{el}). The total interaction energy (V_T) is

experienced by a nanoparticle when approaches another particle, and determines whether the net interaction between the particles is repulsive or attractive (Zhang et al. 2008; Dickson et al. 2012).

DLVO calculations were performed according to the equations described in (Elimelech et al. 1998)):

$$V_{vdw} = \frac{-A}{6}\left[\frac{2R^2}{h(4R+h)} + \frac{2R^2}{(2R+h)^2} + ln\frac{h(4R+h)}{(2R+h)^2}\right] \quad (1)$$

$$V_{el} = 2\pi\varepsilon R\delta^2 ln[1 + e^{-kh}] \quad (2)$$

$$V_T = V_{vdw} + V_{el} \quad (3)$$

where A (J) is the Hamaker constant (1.10^{-9} J for iron nanoparticles (Phenrat et al. 2009)); R (m) is the radius of particles; h (m) is the distance between the surfaces of two interacting particles; $\varepsilon=\varepsilon_r\varepsilon_0$ is the dielectric constant where ε_r (78.54 for water at 25°C) is the relative dielectric constant of the medium and ε_0 ($8.85.10^{-12}$ C^2/J.m) is the permittivity in vacuum; δ, the zeta potential of the charged particles; k (1/m) is the reciprocal of the thickness of the double layer with $k=2.32\times10^9\ (\Sigma C_i Z_i^2)^{1/2}$ where C_i is the concentration of ion, i, and Z_i is its valency value.

The following assumptions/measurements are used in this study:

(1) Particle diameter is 30 nm (average size of the primary particles provided by Sigma Aldrich).

(2) When not specified, ionic strength is assumed to be 1 mM NaCl. In fact, when no electrolytes are used (i.e. when using ultrapure water), equation 2 is reduced to zero and calculations cannot be performed.

(3) Zeta potentials are experimentally determined.

3. Materials and analytical methods

3.1 Chemicals and reagents

Commercially available Fe_2O_3NPs (α-Fe_2O_3, average particle size 30 nm, BET 50-245 m^2/g, 20 wt. % dispersed in water at pH 4), humic acid (HA) (technical grade), NaCl and $CaCl_2$ (99.99% purity) were all supplied by Sigma-Aldrich Australia. HA was employed as a surrogate DOM since HA and more generally humic substances represent an important fraction of DOM in soils, surface and groundwater (Aiken et al. 1985) and have been demonstrated to play a key role in water quality for various pollutants such as trace metals and some organic compounds (Murphy et al. 1990; Maurice and Namjesnik-Dejanovic 1999).

3.2 Sample preparation

Fe_2O_3NPs were suspended in ultrapure water to obtain a set of solutions in the range 10-200 mg/L at pH 4 ± 0.1. Solution pH was adjusted using 0.1 M HCl and 0.1 M NaOH solutions and left for 24 hours to equilibrate, after which the pH was re-measured and adjusted if necessary for all experiments. No

buffers were used in this study because they usually have a high ionic strength and thus may alter the surface chemistry of the Fe_2O_3NPs and enhance their aggregation (Baalousha 2009).

HA was dissolved in ultrapure water with a resistivity of 18 MΩ/cm (MilliQ, Millipore, USA) to obtain a stock solution with a concentration of 500 mg/L. This was then filtered through a 0.45 µm filter using vacuum suction to retain only the 'dissolved' organic matter, and stored at 4°C prior to experimental use. The total organic content (TOC) of the stock solution (dilution 1:10) was measured as 19.1 mgC/L using a TOC analyser (TOC-VCPH, TNM-1, Shimadzu, Japan).

HA-coated Fe_2O_3NPs were prepared by mixing 10 mL of concentrated Fe_2O_3NPs (i.e. 2 g/L) with either 1, 2, 4, 10 or 20 mL of HA (initial concentration of the stock solution: 500 mg/L) for one hour before diluting in ultrapure water to obtain five solutions with Fe_2O_3NP concentration of 200 mg/L and HA concentration of 5, 10, 20, 50 and 100 mg/L. All solutions were then brought to pH 4 ± 0.1 using either 0.1 M HCl or 0.1 M NaOH and stored at 4°C for 24 hours before measurements were taken.

NaCl and $CaCl_2$ were also dissolved in ultrapure water to obtain stock solutions with a concentration of 500 mM. The stock solutions were filtered through a 0.45 µm filter using vacuum suction to avoid dust contamination before being used as the mobile phase in FlFFF experiments or to prepare samples for FlFFF and DLS measurements.

3.3 FlFFF Analysis

FlFFF is a chromatography-like separation technique based on laminar flow (so-called channel flow) in a very thin (i.e. ~250 µm) channel with a cross flow applied perpendicular to the channel flow. The channel flow has a parabolic velocity profile (i.e. the maximum velocity is at the centre of the channel). The cross flow forces the particles to move toward a membrane at the channel wall, from where they can move back into the channel as a result of diffusion forces in the *normal* elution mode (i.e. for particles smaller than 1 µm). The smallest particles, having the highest diffusion coefficient, will migrate farther into the channel at higher flow rates and will thus elute first. The theory and principles of FlFFF can be found elsewhere (Giddings 2000; Phuntsho et al. 2011).

Two different FlFFF systems were used in this study. One was an asymmetrical AF2000 Focus (FlFFFa) (Postnova Analytics, Germany) with channel length of 29.8 cm (tip to tip), channel width of 2 cm and channel thickness of 0.025 cm. The detection system comprised a UV/Vis detector operating at a 254 nm wavelength (SPD 20A from Shimadzu, Japan). The software AF2000 Control, version 1.1.0.23 (Postnova Analytics) was used to control the FlFFF system. A regenerated cellulose membrane (Z-AF4-MEM-612-10KD, Postnova Analytics, Germany) with a molecular weight cut-off of 10 kDa was used as a channel wall. Sodium azide (0.1 mM NH_3) was used as bactericide in the mobile phase for all experiments. The sample volumes were all 20.8 µL and were injected using 50 µL sample loop (Rheodyne Corporation, CA, USA); at least three independent replicates were run per sample and the data averaged. In general, good agreement was observed between replicates (i.e. peak heights differing by less than 5 %). The final solution concentration of Fe_2O_3NPs for all FlFFF/UV experiments was 50 mg/L for the aggregation study and 200 mg/L for the DOM coating stability study to give satisfactory separation and detection. These concentrations are necessary to ensure suitable

detection by UV detectors because the sample becomes considerably diluted in the FlFFF channel during the elution stage.

The second FlFFF system (FlFFFb), used only for the pH effect study, consisted of an Eclipse 3+ system (Wyatt Technology, Dernbach, Germany) with channel length of 26.55 cm (tip to tip) and channel thickness of 0.035 cm, equipped with an Agilent 1200 HPLC system (Agilent technologies, Santa Clara, CA, USA). The Agilent 1200 HPLC system comprised an in-line degasser and an autosampler for the delivery of the carrier liquid and the injection of samples. A regenerated cellulose membrane (Millipore PLGC, 10KD, Wyatt Technology, Dernbach, Germany) with a molecular weight cut-off of 10 kDa was used as a channel wall. The on-line detection system for eluted particles consisted of a UV/Vis absorbance diode array detector (DAD1200, Agilent Technologies) with a spectral range from 190 nm to 950 nm and a quasi-elastic light scattering detector (QELS, Dawn HELEOS II, Wyatt Technology Corporation, Santa Barbara, CA) operating at a wavelength of 658 nm. The software ChemStation, version B.04.02 SP1 (Agilent Technology) was used to control the delivery flow of the FlFFF system. Data acquisition and data processing were done using Astra, version 6.0.2 software (Wyatt Technology). The final solution concentration of Fe_2O_3NPs for all FlFFF/QELS experiments was 200 mg/L since QELS needs relatively high concentrations of particles to ensure proper detection.

3.3.1 FIFFF Calibration Curves

Latex beads of 22 nm, 58 nm, 100 nm and 410 nm were used to create calibration curves from which hydrodynamic diameters of Fe_2O_3NPs were determined. These curves correlate the retention time to particle size. Calibration curves were established for all mobile phases and conditions (change in cross flow or channel flow) used in this study and regularly (i.e. once a week) re-drawn to check the accuracy of sizing. An example of the calibration curves used for the pH effect study can be found in Figure S1.

3.3.2 pH Effect

To investigate the effect of pH on the aggregation of Fe_2O_3NPs samples of 50 mg/L of NPs were pH-adjusted then equilibrated for 24 hours prior to analysis. The mobile phase consisted of ultrapure water prepared at different pH values ranging from pH 3 to pH 10. This is the range of pH tolerance for the FFF membrane; outside this range the membrane may be altered. For pH 2, 11 and 12, only DLS measurements were performed. The FlFFF measurement conditions are summarised in Table 1.

3.3.3 Ionic Strength Effect

The effect of Na^+ and Ca^{2+} on Fe_2O_3NPs aggregation was investigated as follows. NaCl and $CaCl_2$ solutions were prepared at 1mM, 5mM and 10 mM, and 0.5 mM and 2 mM, respectively, by diluting the 500 mM stock solutions using ultrapure water and adjusting to pH 4 before being used as the mobile phase. Fe_2O_3NPs samples of 50 mg/L were suspended in solutions having the same ionic strength as the different mobile phase solutions (i.e. 1 mM, 5 mM and 10 mM NaCl and 0.5 mM and 2 mM $CaCl_2$) and equilibrated for 24 hours before measurements. These ions were chosen because they are abundantly present in soil and in groundwater aquifers in this typical concentration range (Saleh et al. 2008). The operating conditions are presented in Table 1.

230 ### 3.3.4 Stability of DOM-coated Fe_2O_3NPs

231 HA-coated Fe_2O_3NPs at five different HA concentrations were analysed by FlFFF for size
232 determination using ultrapure water at pH 4 as the mobile phase. The operating conditions are
233 displayed in Table 1.
234 The most stable DOM-coated Fe_2O_3NPs (i.e. mixture of 50 mg/L HA and 200 mg/L Fe_2O_3NPs) were
235 then tested under environmentally relevant conditions by modifying the mobile phase and the
236 solution where the particles were suspended (i.e. pH 7, 10 mM NaCl and 0.5 mM $CaCl_2$). The
237 operating conditions are summarised in Table 1.
238 A solution of 100 mg/L of HA was also analysed by FlFFF for molecular weight determination using
239 sodium salt of Polystyrene sulfonates-PSS (Polysciences, Inc., PA, USA) of four different molecular
240 weights (4600, 8000, 18000 and 35000 Da, as provided by the manufacturer, with a polydispersity
241 of 1.1) to create a calibration curve (see Figure S2). The operating conditions were 0.5 mL/min for
242 the channel flow and 3 mL/min for the cross flow.

243 **Table 1**

244 ## 3.4 DLS analysis

245 A Zetasizer (model ZEN3600; Malvern Instruments, Worcestershire, UK) operating with a He-Ne laser
246 at a wavelength of 633 nm was used to determine the zeta potential and hydrodynamic diameter of
247 the different samples. Physical principles, mathematical treatment, and limitations of the DLS data
248 can be found elsewhere (Filella et al. 1997). Samples used in DLS experiments were the same as for
249 FlFFF experiments to ensure data comparability except for the study of concentration effect.

250 ### 3.4.1 Concentration Effect

251 Five solutions of Fe_2O_3NPs were prepared at pH 3 with concentrations of 10, 20, 50, 100 and 200
252 mg/L. The pH was raised slowly from pH 3 to 5 by adding drops of 0.1 M NaOH, and the Z-average
253 hydrodynamic diameter was measured without further modifications. The pH was then brought
254 directly to pH 10 to overcome the aggregation occurring around the PZC, before being raised slowly
255 to pH 12. Finally, solutions were brought from pH 9 to 6 by adding drops of 0.1 M HCl.

256 ## 3.5 Scanning Electron Microscopy (SEM) analysis for the effect of pH

257 Silicon wafers attached on carbon stubs were used for SEM measurements. About 10 µL of sample
258 was deposited on a silicon wafer and left to dry completely. Images were obtained from a Zeiss
259 Supra 55VP variable pressure SEM (Carl Zeiss AG, Germany) and recorded using SmartSEM® software.
260 The mean equivalent circular diameter was determined from these images. Samples used for SEM
261 measurements were the same as those analysed in the FlFFF and DLS experiments for the study of
262 pH effect.

263 # 4. Results and discussions

264 ## 4.1 Characterisation of Fe_2O_3NPs Nanoparticles

265 SEM was used to identify the general characteristics of the Fe_2O_3NPs. At pH 3, the Fe_2O_3NPs were
266 spherical and present as single independent particles, as illustrated in Figure 1a. Analysis of 212

267 particles by SEM yielded a mean equivalent circular diameter of 25 nm with a very low polydispersity
268 (i.e. standard deviation: ± 3.5 nm, Figure 1b).

269 **Figure 1**

270 Zeta potential measurements carried out at different particle concentrations (see Figure S3)
271 suggested that Fe_2O_3NPs are highly positively charged at low pH values (i.e. pH 2-5). The zeta
272 potential decreased as pH increased from 5 to 9 and became highly negative from pH 10 with a PZC
273 at around pH 7 for all particle concentrations. This value is within the range of PZC values (i.e. pH 6.8
274 to 8.1) found in the literature for iron oxide nanoparticles (Tombácz et al. 2004; Illes and Tombácz
275 2006; Baalousha et al. 2008; Baalousha 2009; Hu et al. 2010).

276 4.1.1 Effect of particle concentration on the aggregation behaviour of Fe_2O_3NPs

277 Size measurements by DLS were performed at different particle concentrations ranging from 10 to
278 200 mg/L, and different pH values from pH 2 to 12 (all data are presented in Supportive Table 1). It
279 should be noted that samples with particles having Z-average hydrodynamic diameter > 1,000 nm
280 were settling during the analysis; however, DLS can only be used when particles are strictly
281 subjected to Brownian motion. Thus, these data are only indicative of the agglomeration trend and
282 cannot be used as accurate or absolute measurements.

283 At all particle concentrations, maximum aggregation was reached at the PZC where the net particle
284 surface charge was reduced to zero, as shown in Figure 2. Far from this point, particle aggregate
285 sizes decrease because particles are stabilised by electrostatic repulsion forces.

286 The results also show a particle size concentration dependence at nanoparticle concentrations
287 above 50 mg/L, especially at pH > 5. This is presumably due to the fact that when particle
288 concentration increases, the distance between the particles in the sample is reduced, which
289 increases the chance of collision between particles and hence, their aggregation. Previous studies
290 (Baalousha 2009; Dickson et al. 2012) indicated similar findings for this concentration range. It
291 should be noted here that injected concentrations of Fe_2O_3NPs on contaminated sites are generally
292 between 1 to 10 g/L (Saleh et al. 2008), and aggregation phenomena are expected to be even more
293 exacerbated in this high concentration range.

294 **Figure 2**

295 These results can also be explained by the DLVO theory. Figure 3a and 3b show the interaction
296 forces that arise between two nanoparticles at concentrations of 10 and 200 mg/L, respectively. At
297 10 mg/L and high pH values (i.e. pH 10, 11 and 12), a net positive energy barrier prevents particles
298 from aggregating. Because this barrier decreases from pH 12 to pH 10, we observe an increase in
299 particle aggregate sizes. However, at 200 mg/L and pH 10, the net energy between particles is
300 attractive which induces the aggregation of particles. At pH 11 and pH 12, the net positive barrier,
301 although existing, is too low to prevent the particles from aggregation.

302 **Figure 3**

303 4.1.2 Effect of pH

304 The effect of pH on the aggregate size of Fe_2O_3NPs at a concentration of 50 mg/L is shown in

Table 2 for FlFFFa, DLS and SEM measurements. The results for DLS and FlFFFb measurements at 200 mg/L are reported in Table S1 and S2. The size analysis showed a good agreement among the three measurement techniques. In general, the sizes measured by SEM were comparable to FlFFFa sizes, while the sizes measured by DLS were generally larger than both FlFFFa and FlFFFb. DLS is known to be very sensitive to larger particles and a very small number of large particles (e.g. formed during the aggregation process) can induce a substantial shift toward larger sizes (Domingos et al. 2009). Moreover, it has also been demonstrated that the diffusion coefficient, from which the Z-average hydrodynamic diameter is determined, may show angular dependence and that lower angles yielded more precise values than those obtained at one angle only, which is the case with DLS (Takahashi et al. 2008).

At pH 10, a significant difference in size was observed using the SEM, FlFFF and DLS techniques; the FlFFF results in particular, were much lower than those from other techniques showing the limitation of this technique. This could be explained by the fact that, at this pH, both the FFF membrane and Fe_2O_3NPs are negatively charged. Thus, in addition to the concentration gradient effect that drives the diffusion of particles back into the channel, electrostatic repulsive forces also arise between particles and the membrane, causing lower retention times than expected and translating into an underestimation of particle size.

Another limitation of the FlFFF techniques simulating environmental conditions is related to the recovery of the injected sample. FlFFF fractograms show that the majority of the samples are eluted in the void region (except at pH 3) and only a small fraction of the injected sample (i.e. < 5%) is detected during the elution time. This can probably be explained by the fact that when pH increases, some large aggregates may be formed (> 1 µm). These aggregates (even though not representative of the whole sample) are much larger than the rest of the sample and are eluted in the void peak in *steric* elution mode. To reduce the intensity of the void peak signal, pre-fractionation of the sample could be used to increase the sample concentration and recovery during the elution.

Despite differing in absolute values, size measurements by FlFFF and DLS did show similar trends. Both the hydrodynamic diameter (from FlFFF) and Z-average hydrodynamic diameter (from DLS) increased slightly from pH 3 to 5 with the formation of doublets, triplets or larger aggregates (as illustrated by the SEM images) and then increased significantly at higher pH values, up to a maximum at pH 7 (i.e. at the PZC) with the formation of very large aggregates (cf. SEM image). Around the PZC, aggregation was so extensive that the samples could not be measured by FlFFF and DLS. At pH values above the PZC, aggregate sizes started to decrease but not at the same rate. As discussed previously, at high particle concentration (i.e. 200 mg/L), the chance of collision is enhanced, as is the potential for aggregation due to lower interparticle repulsive forces according to the DLVO theory. However, below 50 mg/L, far from the PZC (i.e. pH 10 to 12), Fe_2O_3NPs remained stable and the average particle size became closer to the original size (i.e. as measured at pH 3).

Table 2

Figure 4 shows the DLVO energy profiles for particle-particle interactions as a function of pH at 50 mg/L. From pH 2 to 7, there is a significant decrease in the repulsive forces between particles due to the decrease in particle surface charge to zero at the PZC (cf. Figure S3). Around the PZC there is no net positive energy barrier promoting the formation of very large aggregates (i.e. up to several

346 micrometres) since the only factor controlling aggregation is Brownian motion (Hu et al. 2010). At
347 higher pH, starting at pH 10, the particles become highly negatively charged; giving rise to repulsive
348 forces, and a net positive energy barrier once again prevents particles from aggregating.

349 **Figure 4**

350 4.1.3 Effect of ionic strength

351 Figure 5 shows the FlFFF/UV fractograms of Fe_2O_3NPs as a function of ionic strength, and Table 3
352 gives the corresponding hydrodynamic diameters obtained from the FFF fractograms as well as the
353 Z-average hydrodynamic diameters obtained by DLS measurements.

354 The DLS results show an increase in particle aggregate sizes with increasing ionic strength. At low
355 ionic strength (1 mM-5 mM NaCl and 0.5 mM $CaCl_2$), the Z-average hydrodynamic diameter varies
356 slightly from 63.19 to 64.92 nm. This is not significantly different from the size of nanoparticles
357 measured in ultrapure water. This indicates that at low ionic strength, electrostatic repulsive forces
358 are dominant over the attractive forces, preventing particles from aggregation. However, the use of
359 10 mM NaCl or 2 mM $CaCl_2$ resulted in particle aggregation, probably due to the reduction in
360 repulsive forces between particles as shown in Figure 6.

361 The FlFFF fractograms (Figure 5) show no change in the retention times with increased ionic strength
362 but a significant decrease in the UV signal intensity is observed. The constant elution time is
363 expected as it has been demonstrated in previous studies that ionic strength has no effect on
364 retention time of particles of the same size (Dubascoux et al. 2008; Shon et al. 2009).

365 **Figure 5**

366 **Table 3**

367 However, the decrease in UV signal points to a lower recovery at higher ionic strength, which could
368 be explained by the DLVO theory and DLS results. Figure 6 shows that increasing ionic strength leads
369 to a significant decrease in the repulsive forces between particles, which could lead to the formation
370 of larger particle aggregates. Dubascoux et al. (2008) explained that an increase in ionic strength
371 leads to a decrease in the double layer thickness of particles, which promotes the formation of larger
372 aggregates. These larger clusters of particles will be located closer to the FFF membrane which will
373 increase the interactions between the membrane and these larger aggregates. Thus, they could be
374 irreversibly adsorbed onto the membrane explaining the observed decrease in the UV signal.

375 **Figure 6**

376 4.2 Stability of DOM-coated Fe_2O_3NPs under environmentally relevant
377 conditions

378 4.2.1 Effect of DOM on particle charge

379 Figure 7 shows the zeta potential profiles of Fe_2O_3NPs alone (200 mg/L), HA-coated Fe_2O_3NPs at
380 variable HA concentration and HA alone (50 mg/L) plotted as a function of pH, ranging from 3 to 10.

381 At low HA concentrations (i.e. from 5 to 20 mg/L), the zeta potential of Fe_2O_3NPs decreases,
382 resulting in the PZC occurring at lower pH values (i.e. from pH 7 for 0 mg/L HA to pH 4 for 20 mg/L
383 HA). This shift in the pH of the PZC is probably due to the adsorption of HA on the surface of
384 Fe_2O_3NPs causing a change in their surface charge. The zeta potential of HA indicates that it is
385 negatively charged over the whole pH range. This is due to the fact that HA macromolecules carry
386 many functional groups, including carboxylic and phenolic groups (Hajdú et al. 2009; Hu et al. 2010;
387 Dickson et al. 2012). At concentrations above 20 mg/L, the zeta potential of HA-coated Fe_2O_3NPs
388 remained negative across the whole pH range tested. At pH values greater than the PZC of the
389 uncoated Fe_2O_3NPs, both Fe_2O_3NPs and HA are negatively charged and adsorption of HA is not
390 expected to occur. Thus, the decrease in zeta potential values is probably due to the increased HA
391 concentration which brings more negative charges into solution and shifts the zeta potential
392 downwards.

393 **Figure 7**

394 ### 4.2.2 Effect of DOM concentration on particle aggregation

395 The effect of HA concentration on the aggregation of HA-coated Fe_2O_3NPs was investigated by FlFFF
396 and DLS (Figure 8 a and b) at pH 4. At this pH, Fe_2O_3NPs are strongly positively charged (i.e. zeta
397 potential of +38.5 mV, Figure 7) and HA is still strongly negatively charged (i.e. zeta potential of -38.8
398 mV, Figure 7). As the adsorption of DOM on the surface of Fe_2O_3NPs is mainly governed by
399 Coulombic interactions via ligand-exchange reactions, this provides the most favourable conditions
400 for sorption (Filius et al. 2000; Chorover and Amistadi 2001; Illés and Tombácz 2004).

401 At low concentration (i.e. < 20 mgHA/L), HA partially neutralises the positive charges on Fe_2O_3NPs as
402 shown in the zeta potential profile in Figure 7. Thus, aggregation takes place and extends with
403 increasing HA concentration to reach a peak at 20 mgHA/L at which point the zeta potential is
404 reduced to almost zero. At HA concentrations of 10 and 20 mg/L, very large aggregates were formed
405 (see Figure 8 b) and due to their rapid sedimentation on the bottom of the vial, FlFFF analysis could
406 not be performed. From the FlFFF fractogram of the mixture of Fe_2O_3NPs with 5 mg/L of HA, the
407 following observations can be made. Compared to the fractogram of Fe_2O_3NPs alone, there is a slight
408 increase in the void peak UV signal which is probably due to the loss of sample during the injection
409 and focusing step and because HA is better adsorbed by UV as shown on the fractogram of HA alone.
410 The second observation is that no apparent shift toward larger retention times is observed because
411 the difference in size obtained from both fractograms is very low. This can be explained by the fact
412 that at 5 mgHA/L, there is a very low amount of HA in the solution; thus, the number of coated
413 nanoparticles is very low and they were not detected during the FFF analysis.

414 **Figure 8**

415 At higher HA concentrations (i.e. ≥ 50 mg/L), the surface of the Fe_2O_3NPs becomes negatively
416 charged (i.e. -27.1 mV at 50 mgHA/L, Figure 7) providing electrostatic stabilisation of the particles
417 and reducing their aggregation (i.e. from almost 1700 nm at 20 mgHA/L to 85.2 nm at 50 mgHA/L as
418 measured by DLS as shown in Figure 8 b). A significant increase in the void peak UV signal can be
419 observed on the FFF fractograms of 50 mgHA/L and 100 mgHA/L (Figure 8 a). This can be caused by
420 the unadsorbed HA macromolecules. In fact, HA has a molecular weight of 38.7 kDa (as measured by
421 FlFFF – see Figure S4) which corresponds to approximately 1.7 nm (conversion based on (Shon et al.

2006)) and is considerably smaller than the Fe_2O_3NPs. Therefore, the applied cross flow was too low to retain the unadsorbed HA molecules, and the elution of unretained HA is indicated by the larger void peak. FFF results also showed a shift toward higher retention times (compared to the FIFFF fractogram of bare Fe_2O_3NPs), indicating the formation of small aggregates of coated-particles. The broadening of the peak is probably caused by aggregates having different size and conformation. At a HA concentration of 100 mg/L, both DLS and FFF measurements indicate an increase in the particle size, which is probably due to the formation of larger aggregates. This consideration is supported by the fact that a small fraction of the sample settled on the bottom of the vial.

Finally, by comparing DLS and FFF results, it is clear that FFF, as a fractionation method, can provide not only the hydrodynamic diameter of the coated particles but also valuable information on the coating itself. For instance, the FFF results may be used to assess the amount of HA coated onto the nanoparticles by comparing the intensity of the void peak on the fractograms of HA alone and HA-coated Fe_2O_3NPs. This demonstrates the versatility of FFF over conventional size-measurement techniques.

4.2.3 Stability under realistic conditions of pH and ionic composition

The stability of HA-coated Fe_2O_3NPs was tested under realistic environmental conditions (i.e. pH 7, 10 mM NaCl and 0.5 mM $CaCl_2$) to verify whether or not this coating could be used effectively in the field. Figure 9 shows the FFF and DLS results for the stability study of a mixture of Fe_2O_3NPs (200 mg/L) coated by HA (50 mg/L).

Compared to bare Fe_2O_3NPs, HA-coated Fe_2O_3NPs were less affected by an increase in pH and were much more stable under neutral pH conditions. In fact, for the bare nanoparticles, an increase in pH to pH 7 (i.e. the PZC) resulted in extensive aggregation with the formation of large aggregates that were thirty-five times larger than at pH 4 (Figure 9b). However, when the nanoparticles were coated with HA, the same increase in pH resulted in a size increase of less than 15%. This is most likely due to the negatively charged HA layer on the Fe_2O_3NPs surface which prevents particles from aggregating through electrostatic repulsion. Moreover, the macromolecular layer can also provide steric stabilisation by causing entropically unfavourable conditions when the particles come closer to one another (Tiller and O'Melia 1993; Illés and Tombácz 2004).

Figure 9

Regarding the effect of NaCl on the stability of HA-coated Fe_2O_3NPs, FFF and DLS results (cf. Figure 9) showed that increasing the NaCl concentration to 10 mM does not result in aggregation or sedimentation of the sample in comparison to bare Fe_2O_3NPs. In fact, it has been demonstrated in previous studies (Illés and Tombácz 2004; Hajdú et al. 2009) that HA-coated Fe_2O_3NPs are more stable under high NaCl concentration due to the electrosteric stabilisation providing by HA coating.

In the presence of $CaCl_2$ at 0.5 mM, HA-coated Fe_2O_3NPs became unstable and formed large aggregates (greater than 500 nm when measured by DLS). The effect of increasing the $CaCl_2$ concentration on FFF results is that no peaks were observed, which is most likely to be the results of aggregation and consequently much longer retention times. This aggregation behaviour could be attributed to the formation of complexes between Ca^{2+} and HA, which neutralises the negative charge imparted by the HA coating on the Fe_2O_3NPs and thus, reduces the electrostatic stabilisation

which previously arose between the coated nanoparticles. In addition, the presence of Ca^{2+} cations may promote the formation of complexes Fe_2O_3NPs-HA-Ca^{2+}-HA- Fe_2O_3NPs (Chen et al. 2006). It has also been reported that other alkaline earth metal divalent cations such Ba^{2+} and Sr^{2+} could accelerate hematite aggregate growth at very low concentrations, whereas Mg^{2+} showed no effect on aggregation even at high concentrations (Chen et al. 2007).

5. Conclusions

The stability of both coated and uncoated Fe_2O_3NPs has been investigated under different environmental conditions by using several analytical techniques and a theoretical method. The need for a multi-method approach has been demonstrated by highlighting the limitations of each method. For instance, one of the limitations of DLS is the polydispersity of the sample which leads to an over-estimation of the average particle size. With FFF, limitations arise from the interaction between the membrane and the particles; furthermore the pH dependent changes in the surface charge of the NPs, which controls the interaction with membrane, may limit the suitability of latex beads as references for particle size. Therefore, the use of FFF with mobile phases mimicking environmentally relevant conditions may not provide definitive answers in terms of particle size as in this case most measurements will not be made using an optimised mode of operation. However, the versatility of FFF was demonstrated for the characterisation of HA-coated Fe_2O_3NPs by providing valuable information on the adsorption of HA onto Fe_2O_3NPs. Finally, the DLVO modelling approach is useful for the interpretation of the experimental results, but cannot predict the size of the aggregates. The presence of large aggregates (i.e. above 1 µm) and sedimentation of these aggregates during the analysis were also a significant limitation to the collection of accurate and reliable data. Therefore, this study shows that it is essential to deploy a number of analytical and theoretical techniques to investigate the behaviour of NPs. Other analytical methods that can measure the size of aggregates in this size range with greater accuracy (e.g. low-angle laser light scattering (LALLS) techniques) should also be considered.

The pH and ionic strength are important environment conditions that need to be carefully considered before releasing nanoparticles into the environment. In the case of Fe_2O_3NPs, commonly encountered soil and groundwater conditions (i.e. pH 6-8 and high ionic strength) can induce extensive aggregation and can thus considerably reduce their mobility and reactivity once injected into subsurface environments. Finding solutions to reduce or suppress particle aggregation is therefore crucial in optimising remediation strategies using these materials. Surface coating is one of the preferred methods used to enhance the stability of the Fe_2O_3NPs. The choice of surface modifier is important and this will depend on the soil conditions and the target contaminants. This study has demonstrated the performance of DOM as a surface coating under conditions similar to the natural soil environment. DOM-coated nanoparticles were observed to show higher stability than naked Fe_2O_3NPs under some conditions. Aggregation and stabilisation have significant effects on the environmental transport, reactivity and fate of the released nanoparticles and especially on the transport of low-solubility contaminants in subsurface waters. Increased stabilisation will result in better transport and reactivity in the subsurface but may also increase contaminant transportation. Development of modellings on the behaviour of MNPs in the subsurface is still needed but restrained by the lack of data under relevant environmental conditions.

Acknowledgements

This research was funded by the Cooperative Research Centre for Contamination Assessment and Remediation of the Environment (CRC CARE). Enzo Lombi acknowledges the Australian Research Council's support through a Future Fellowship grant (FT100100337).

References

Aiken, G. R., D. M. McKnight, et al. (1985). Humic substances in soil, sediment, and water: geochemistry, isolation and characterization, John Wiley & Sons.

Alowitz, M. J. and M. M. Scherer (2002). "Kinetics of nitrate, nitrite, and Cr(vi) reduction by iron metal." Environmental Science and Technology **36**(3): 299-306.

Baalousha, M. (2009). "Aggregation and disaggregation of iron oxide nanoparticles: Influence of particle concentration, pH and natural organic matter." Science of the Total Environment **407**(6): 2093-2101.

Baalousha, M., A. Manciulea, et al. (2008). "Aggregation and surface properties of iron oxide nanoparticles: Influence of pH and natural organic matter." Environmental Toxicology and Chemistry **27**(9): 1875-1882.

Chen, J., Z. Xiu, et al. (2011). "Effect of natural organic matter on toxicity and reactivity of nano-scale zero-valent iron." Water Research **45**(5): 1995-2001.

Chen, K. L., S. E. Mylon, et al. (2006). "Aggregation kinetics of alginate-coated hematite nanoparticles in monovalent and divalent electrolytes." Environmental science & technology **40**(5): 1516-1523.

Chen, K. L., S. E. Mylon, et al. (2007). "Enhanced aggregation of alginate-coated iron oxide (hematite) nanoparticles in the presence of calcium, strontium, and barium cations." Langmuir **23**(11): 5920-5928.

Chorover, J. and M. K. Amistadi (2001). "Reaction of forest floor organic matter at goethite, birnessite and smectite surfaces." Geochimica et Cosmochimica Acta **65**(1): 95-109.

Cirtiu, C. M., T. Raychoudhury, et al. (2011). "Systematic comparison of the size, surface characteristics and colloidal stability of zero valent iron nanoparticles pre- and post-grafted with common polymers." Colloids and Surfaces A: Physicochemical and Engineering Aspects **390**(1-3): 95-104.

Crane, R. A. and T. B. Scott (2012). "Nanoscale zero-valent iron: Future prospects for an emerging water treatment technology." Journal of Hazardous Materials **211-212**: 112-125.

Derjaguin, B. and L. Landau (1941). "Theory of the stability of strongly charged lyophobic sols and of the adhesion of strongly charged particles in solutions of electrolytes." Acta Physicochim URSS **14**(6): 633-662.

Dickson, D., G. Liu, et al. (2012). "Dispersion and stability of bare hematite nanoparticles: Effect of dispersion tools, nanoparticle concentration, humic acid and ionic strength." Science of the Total Environment **419**(0): 170-177.

Domingos, R. F., M. A. Baalousha, et al. (2009). "Characterizing manufactured nanoparticles in the environment: multimethod determination of particle sizes." Environmental science & technology **43**(19): 7277-7284.

Dubascoux, S., F. Von Der Kammer, et al. (2008). "Optimisation of asymmetrical flow field flow fractionation for environmental nanoparticles separation." Journal of Chromatography A **1206**(2): 160-165.

Elimelech, M., X. Jia, et al. (1998). Particle deposition and aggregation: measurement, modelling and simulation Woburn, Massachusetts Butterworth-Heinemann 440.

Elliott, D. W. and W. X. Zhang (2001). "Field assessment of nanoscale bimetallic particles for groundwater treatment." Environmental Science and Technology **35**(24): 4922-4926.

Filella, M., J. Zhang, et al. (1997). "Analytical applications of photon correlation spectroscopy for size distribution measurements of natural colloidal suspensions: capabilities and limitations." Colloids and Surfaces A: Physicochemical and Engineering Aspects **120**(1): 27-46.

Filius, J. D., D. G. Lumsdon, et al. (2000). "Adsorption of fulvic acid on goethite." Geochimica et Cosmochimica Acta **64**(1): 51-60.

Giddings, J. C. (2000). Field flow fractionation handbook Chapter 1: The field-flow fractionation family: Underlying principles, Wiley-interscience.

Hajdú, A., E. Illés, et al. (2009). "Surface charging, polyanionic coating and colloid stability of magnetite nanoparticles." Colloids and Surfaces A: Physicochemical and Engineering Aspects **347**(1–3): 104-108.

Hassellöv, M. and R. Kaegi (2009). Environmental and Human Health Effects of Nanoparticles. Chichester, Wiley.

He, F. and D. Zhao (2007). "Manipulating the size and dispersibility of zerovalent iron nanoparticles by use of carboxymethyl cellulose stabilizers." Environmental Science and Technology **41**(17): 6216-6221.

He, F., D. Zhao, et al. (2007). "Stabilization of Fe - Pd nanoparticles with sodium carboxymethyl cellulose for enhanced transport and dechlorination of trichloroethylene in soil and groundwater." Industrial and Engineering Chemistry Research **46**(1): 29-34.

He, Y. T., J. Wan, et al. (2008). "Kinetic stability of hematite nanoparticles: the effect of particle sizes." Journal of Nanoparticle Research **10**(2): 321-332.

Hong, S. and M. Elimelech (1997). "Chemical and physical aspects of natural organic matter (NOM) fouling of nanofiltration membranes." Journal of Membrane Science **132**(2): 159-181.

Hu, J.-D., Y. Zevi, et al. (2010). "Effect of dissolved organic matter on the stability of magnetite nanoparticles under different pH and ionic strength conditions." Science of the Total Environment **408**(16): 3477-3489.

Illes, E. and E. Tombácz (2006). "The effect of humic acid adsorption on pH-dependent surface charging and aggregation of magnetite nanoparticles." Journal of Colloid and Interface Science **295**(1): 115-123.

Illés, E. and E. Tombácz (2004). "The role of variable surface charge and surface complexation in the adsorption of humic acid on magnetite." Colloids and Surfaces A: Physicochemical and Engineering Aspects **230**(1–3): 99-109.

Jortner, J. and C. N. R. Rao (2002). "Nanostructured advanced materials. Perspectives and directions." Pure and Applied Chemistry **74**(9): 1491-1506.

Kanel, S. R., B. Manning, et al. (2005). "Removal of arsenic(III) from groundwater by nanoscale zero-valent iron." Environmental Science and Technology **39**(5): 1291-1298.

Lead, J. R. and K. J. Wilkinson (2006). "Aquatic colloids and nanoparticles: current knowledge and future trends." Environmental Chemistry **3**(3): 159-171.

Liu, J., Z. Zhao, et al. (2008). "Coating Fe3O4 magnetic nanoparticles with humic acid for high efficient removal of heavy metals in water." Environmental Science & Technology **42**(18): 6949-6954.

Liu, Y., S. A. Majetich, et al. (2005). "TCE dechlorination rates, pathways, and efficiency of nanoscale iron particles with different properties." Environmental Science and Technology **39**(5): 1338-1345.

Maurice, P. and K. Namjesnik-Dejanovic (1999). "Aggregate structures of sorbed humic substances observed in aqueous solution." Environmental Science & Technology **33**(9): 1538-1541.

Murphy, E. M., J. M. Zachara, et al. (1990). "Influence of mineral-bound humic substances on the sorption of hydrophobic organic compounds." Environmental science & technology **24**(10): 1507-1516.

Mylon, S. E., K. L. Chen, et al. (2004). "Influence of natural organic matter and ionic composition on the kinetics and structure of hematite colloid aggregation: Implications to iron depletion in estuaries." Langmuir **20**(21): 9000-9006.

Phenrat, T., H. J. Kim, et al. (2009). "Particle size distribution, concentration, and magnetic attraction affect transport of polymer-modified Fe0 nanoparticles in sand columns." Environmental Science & Technology **43**(13): 5079-5085.

Phenrat, T., G. Lowry, et al. (2009). "Physicochemistry of polyelectrolyte coatings that increase stability, mobility, and contaminant specificity of reactive nanoparticles used for groundwater remediation." Nanotechnology Applications for Clean Water: 249-267.

Phenrat, T., N. Saleh, et al. (2007). "Aggregation and sedimentation of aqueous nanoscale zerovalent iron dispersions." Environmental Science and Technology **41**(1): 284-290.

Phuntsho, S., H. Shon, et al. (2011). "Assessing membrane fouling potential of humic acid using flow field-flow fractionation." Journal of Membrane Science **373**(1-2): 64-73.

Ponder, S. M., J. G. Darab, et al. (2000). "Remediation of Cr(VI) and Pb(II) aqueous solutions using supported, nanoscale zero-valent iron." Environmental Science and Technology **34**(12): 2564-2569.

Quinn, J., C. Geiger, et al. (2005). "Field demonstration of DNAPL dehalogenation using emulsified zero-valent iron." Environmental Science and Technology **39**(5): 1309-1318.

Saleh, N., H. J. Kim, et al. (2008). "Ionic strength and composition affect the mobility of surface-modified Fe0 nanoparticles in water-saturated sand columns." Environmental Science & Technology **42**(9): 3349-3355.

Saleh, N., T. Phenrat, et al. (2005). "Adsorbed triblock copolymers deliver reactive iron nanoparticles to the oil/water interface." Nano letters **5**(12): 2489-2494.

Saleh, N., K. Sirk, et al. (2007). "Surface modifications enhance nanoiron transport and NAPL targeting in saturated porous media." Environmental Engineering Science **24**(1): 45-57.

Schrick, B., B. W. Hydutsky, et al. (2004). "Delivery vehicles for zerovalent metal nanoparticles in soil and groundwater." Chemistry of Materials **16**(11): 2187-2193.

Shon, H. K., S. Puntsho, et al. (2009). "A study on the influence of ionic strength on the elution behaviour of membrane organic foulant using advanced separation tools." Desalination and Water Treatment **11**(1-3): 38-45.

Shon, H. K., S. Vigneswaran, et al. (2006). "Effect of partial flocculation and adsorption as pretreatment to ultrafiltration." AIChE Journal **52**(1): 207-216.

Sirk, K. M., N. B. Saleh, et al. (2009). "Effect of adsorbed polyelectrolytes on nanoscale zero valent iron particle attachment to soil surface models." Environmental Science & Technology **43**(10): 3803-3808.

Sun, Y.-P., X.-q. Li, et al. (2006). "Characterization of zero-valent iron nanoparticles." Advances in Colloid and Interface Science **120**(13): 47-56.

Takahashi, K., H. Kato, et al. (2008). "Precise measurement of the size of nanoparticles by dynamic light scattering with uncertainty analysis." Particle & Particle Systems Characterization **25**(1): 31-38.

Tiller, C. L. and C. R. O'Melia (1993). "Natural organic matter and colloidal stability: Models and measurements." Colloids and Surfaces A: Physicochemical and Engineering Aspects **73**(0): 89-102.

Tiraferri, A., K. L. Chen, et al. (2008). "Reduced aggregation and sedimentation of zero-valent iron nanoparticles in the presence of guar gum." Journal of Colloid and Interface Science **324**(1-2): 71-79.

Tombácz, E., Z. Libor, et al. (2004). "The role of reactive surface sites and complexation by humic acids in the interaction of clay mineral and iron oxide particles." Organic Geochemistry **35**(3): 257-267.

Verwey, E. and J. T. G. Overbeek (1948). "Theory of the stability of lyophobic colloids." Amserdam: Elsevier.

Verwey, E. J. W. (1947). "Theory of the stability of lyophobic colloids." The Journal of Physical Chemistry **51**(3): 631-636.

Wang, C.-B. and W.-X. Zhang (1997). "Synthesizing nanoscale iron particles for rapid and complete dechlorination of TCE and PCBs." Environmental Science & Technology **31**(7): 2154-2156.

Zhang, W.-X. (2003). "Nanoscale iron particles for environmental remediation: An overview." Journal of Nanoparticle Research **5**: 323-332.

Zhang, W.-x., C.-B. Wang, et al. (1998). "Treatment of chlorinated organic contaminants with nanoscale bimetallic particles." Catalysis Today **40**(4): 387-395.

Zhang, Y., Y. Chen, et al. (2008). "Stability of commercial metal oxide nanoparticles in water." Water Research **42**(8-9): 2204-2212.

712 # LIST OF FIGURES

713

730

Figure 1

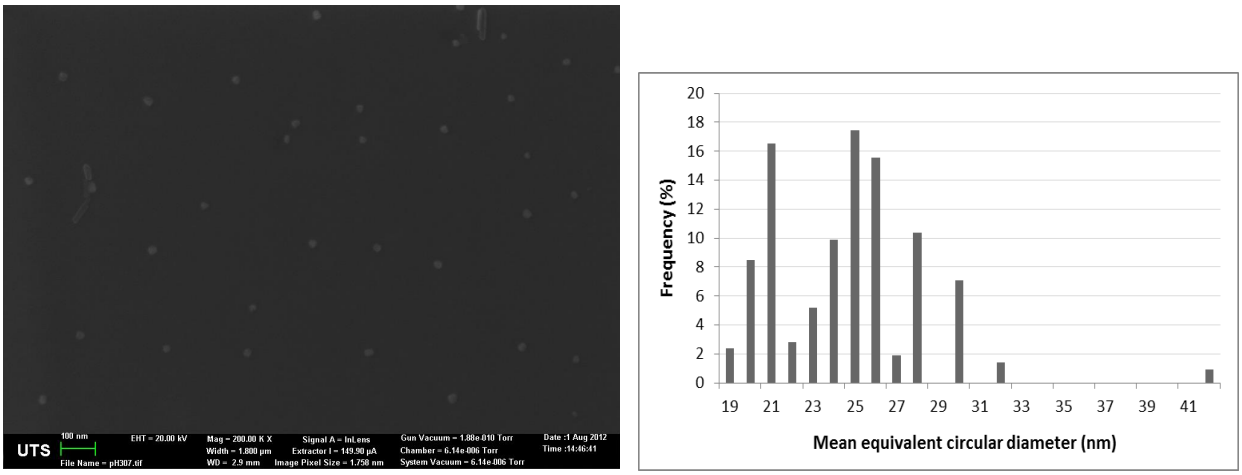

a) b)

Figure 2

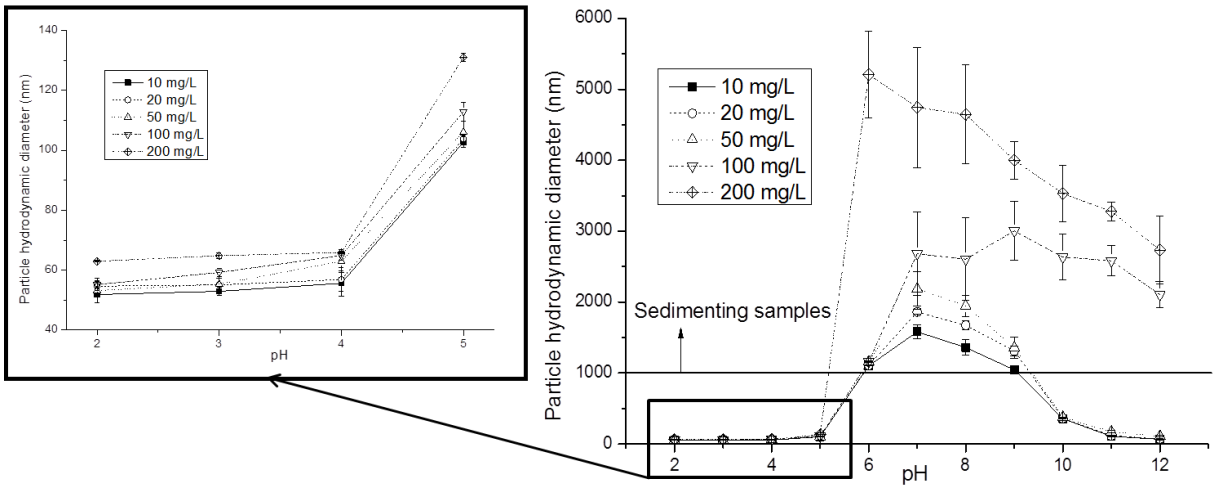

Figure 3

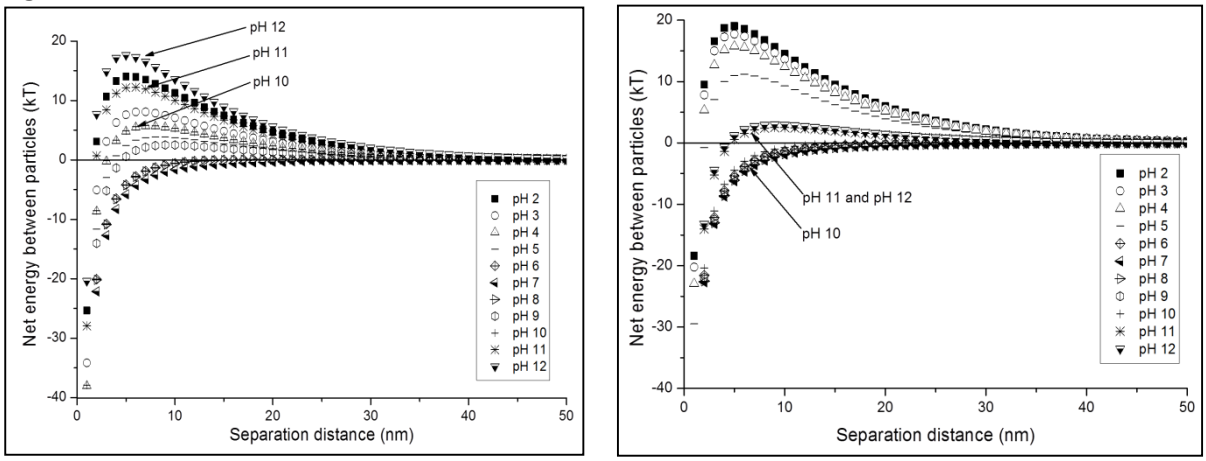

a) b)

Figure 4

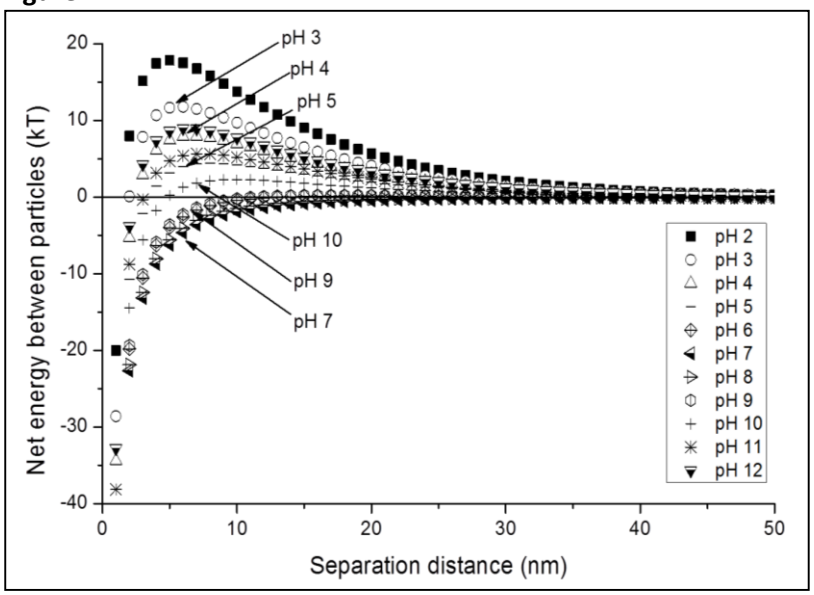

Figure 5

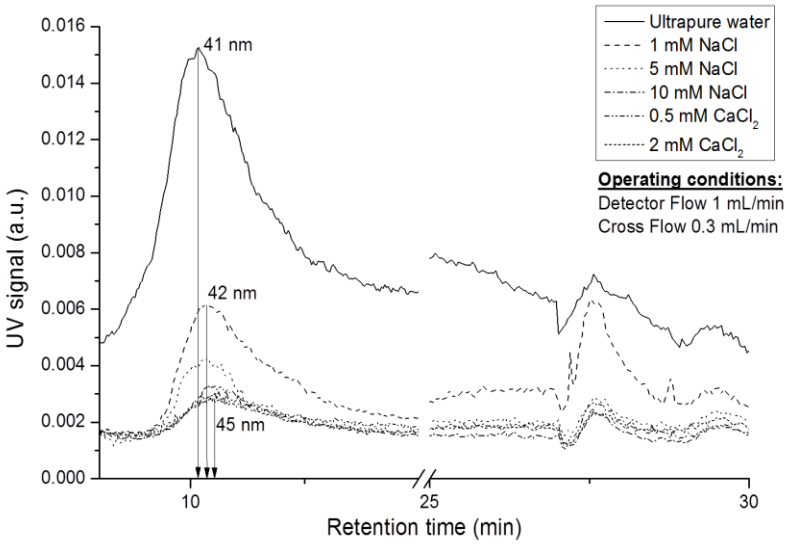

Figure 6

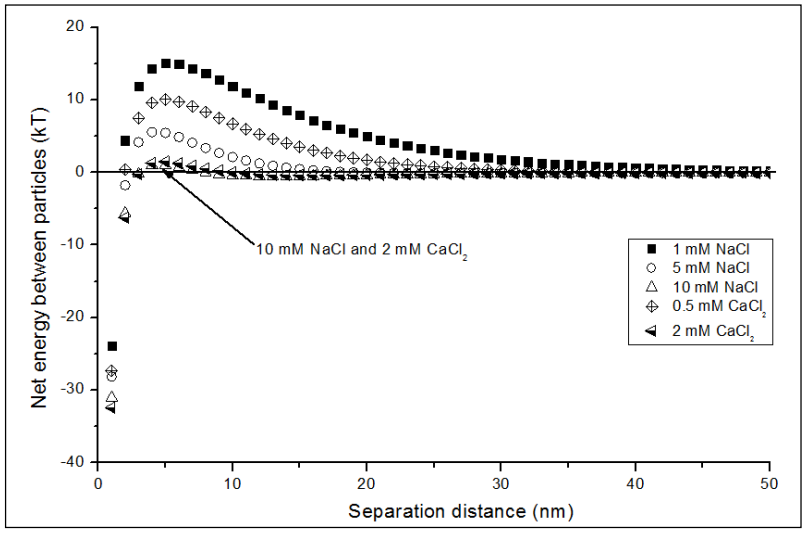

Figure 7

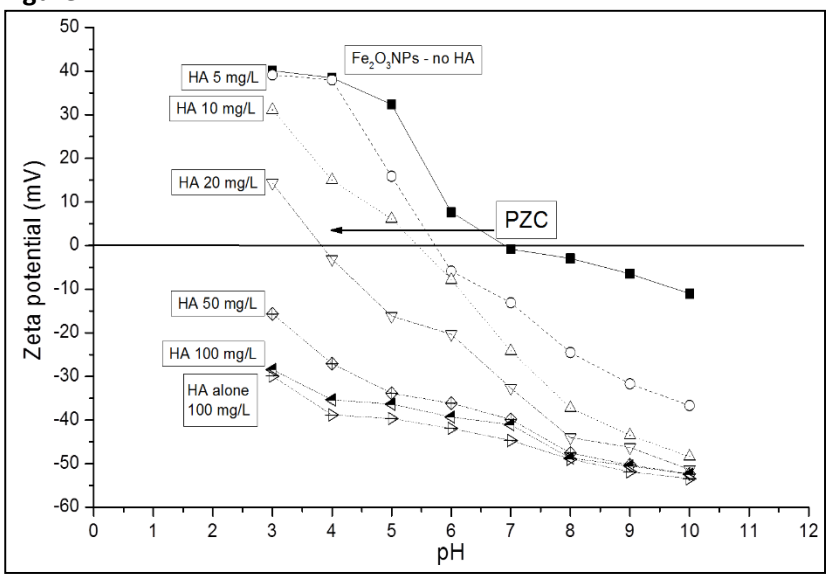

Figure 8

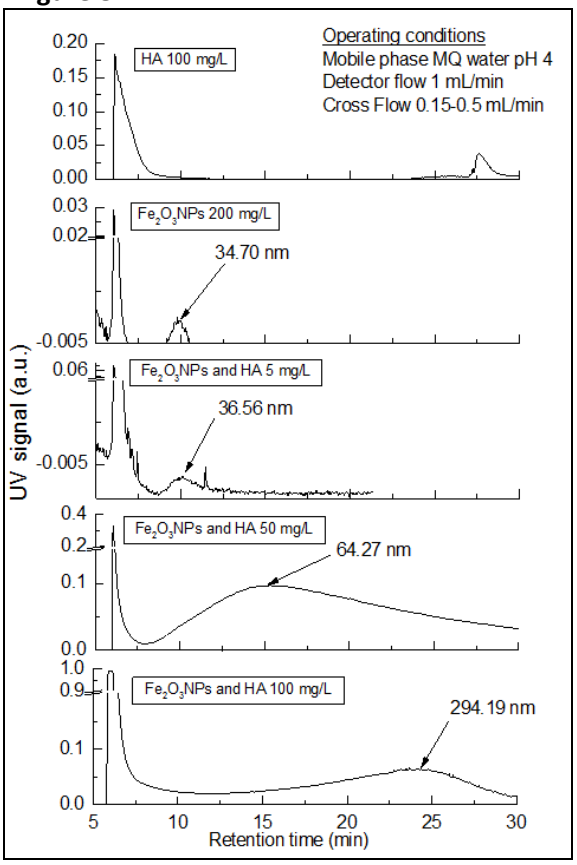

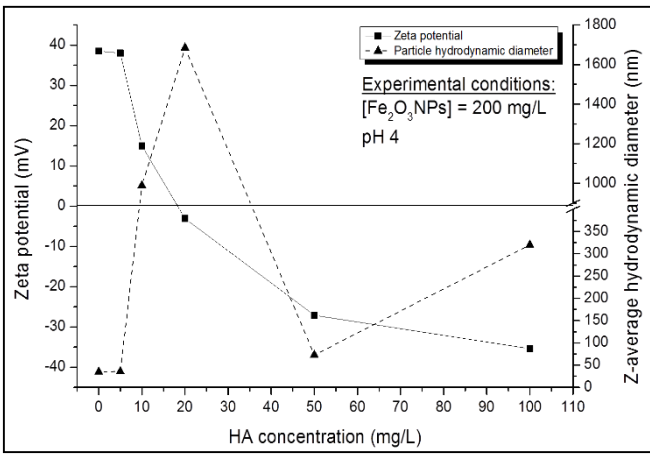

a) b)

Figure 9

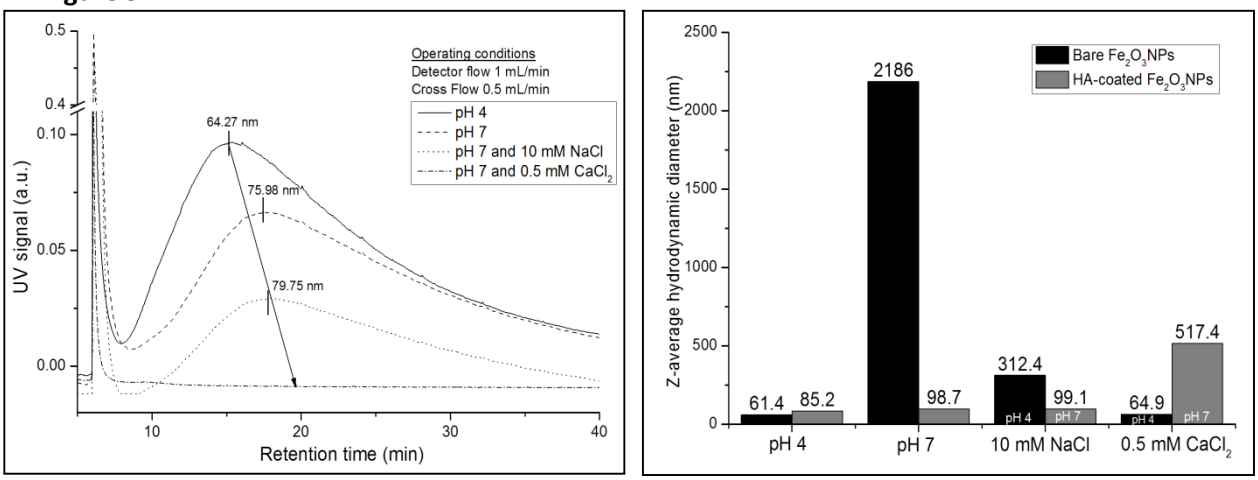
Operating conditions
Detector flow 1 mL/min
Cross Flow 0.5 mL/min
pH 4
pH 7
pH 7 and 10 mM NaCl
pH 7 and 0.5 mM CaCl2
64.27 nm
75.98 nm
79.75 nm
UV signal (a.u.)
Retention time (min)
Bare Fe2O3NPs
HA-coated Fe2O3NPs
Z-average hydrodynamic diameter (nm)
61.4
85.2
2186
98.7
312.4
99.1
64.9
517.4
pH 4
pH 7
10 mM NaCl
0.5 mM CaCl2

a) b)

754

755 # LIST OF TABLES

756

762

763

764 **Table 1**

Study		Channel Flow (mL/min)	Cross Flow (mL/min)	Mobile phase
1. Effect of pH	pH 3	1	0.5	Ultrapure water at pH 3
	pH 4		0.3	Ultrapure water at pH 4
	pH 5		0.15	Ultrapure water at pH 5
	pH 10			Ultrapure water at pH 10
2. Effect of Ionic Strength	Ultrapure water	1	0.3	Ultrapure water at pH 4
	1 mM NaCl			1 mM NaCl at pH 4
	5 mM NaCl			5 mM NaCl at pH 4
	10 mM NaCl			10 mM NaCl at pH 4
	0.5 mM $CaCl_2$			0.5 mM $CaCl_2$ at pH 4
	2 mM $CaCl_2$			2 mM $CaCl_2$ at pH 4
3. Effect of HA concentration	HA alone (100 mg/L)	1	0.5	Ultrapure water at pH 4
	Fe_2O_3NPs alone (200 mg/L)			
	HA/Fe_2O_3NPs 5 mgHA/L			
	HA/Fe_2O_3NPs 50 mgHA/L			
	HA/Fe_2O_3NPs 100 mgHA/L		0.15	
4. Stability of HA-coated Fe_2O_3NPs	pH 4	1	0.5	Ultrapure water at pH 4
	pH 7			Ultrapure water at pH 7
	pH 7/10 mM NaCl			10 mM NaCl at pH 7
	pH 7/0.5 mM $CaCl_2$			0.5 mM $CaCl_2$ at pH 7

765

766

767 **Table 2**

pH	FlFFF/UV fractograms and hydrodynamic diameter (nm)	Z-average hydrodynamic diameter as determined by DLS (nm)	Corresponding SEM images (50 mg/L)
3	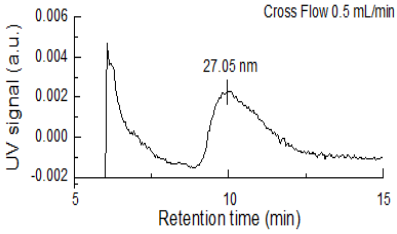 27.05 ± 0.16	55.3 ± 2.4	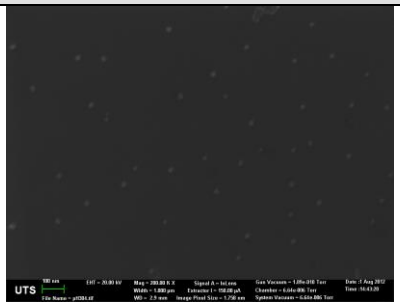 Approximated size: 25 nm
4	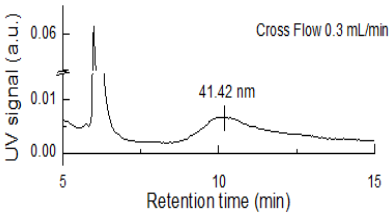 41.42 ± 0.04	63.0 ± 3.9	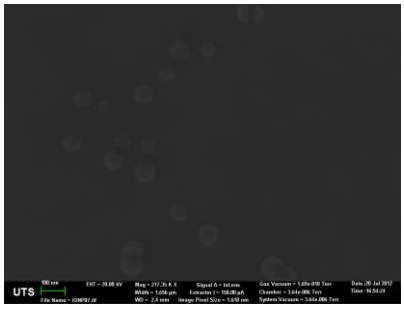 Approximated size: 35 nm
5	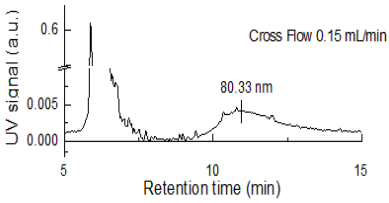 80.33 ± 0.74	106.1 ± 3.6	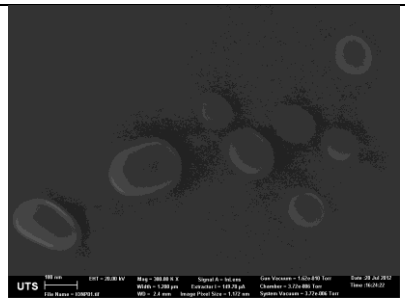 Approximated size: 80 nm
7	Samples settled down rapidly to the bottom of the vial and could not be analysed by FlFFF and DLS.		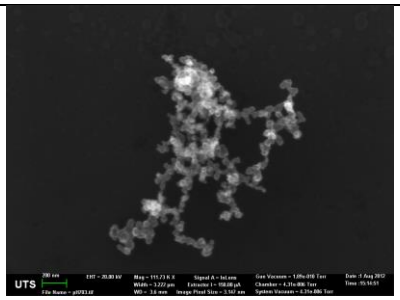 Approximated size: 1500 nm
10	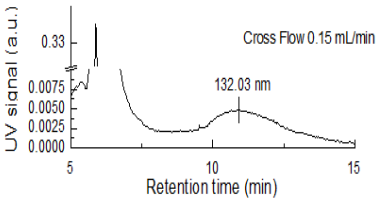 132.03 ± 5.85	377.5 ± 3.6	 Approximated size: 250 nm

768

769 **Table 3**

Ionic strength	Particle size (nm)	
	FlFFF/UV	**DLS**
Ultrapure water	41.4 ± 0.1	61.4 ± 1.4
1 mM NaCl	42.3 ± 0.1	63.2 ± 3.6
5 mM NaCl	42.8 ± 1.7	64.4 ± 5.2
10 mM NaCl	44.7 ± 2.5	312.4 ± 10.7
0.5 mM $CaCl_2$	44.4 ± 0.6	64.9 ± 4.9
2 mM $CaCl_2$	44.8 ± 2.7	438.7 ± 18.1

770

771